Int. J. Heat Mass Transfer. Vol. 33, No. 4, pp. 583–591, 1990
Printed in Great Britain

0017–9310/90 $3.00 + 0.00
© 1990 Pergamon Press plc

Pressure drop characteristics for turbulent flow in a straight circular tube situated downstream of a bend

M. M. OHADI,† E. M. SPARROW,‡ A. WALAVALKAR† and A. I. ANSARI†

† Mechanical Engineering–Engineering Mechanics Department, Michigan Technological University, Houghton, MI 49931, U.S.A.

‡ Mechanical Engineering Department, University of Minnesota, Minneapolis, MN 55455, U.S.A.

(*Received* 30 *March* 1989 *and in final form* 23 *June* 1989)

Abstract—Experiments are performed to quantify the effects of a bend on the pressure distributions and friction factors in a straight tube situated downstream of a bend. Results are reported for parametric values of the Reynolds number (5000–80 000), bend turn angle (0, 90, and 180 deg), and the flow delivery configuration at the inlet of the bend (either a hydrodynamic development tube or a sharp-edged inlet). The 0 deg turn angle corresponds to the no-bend case, which serves as a baseline against which the with-bend cases are compared. It is found that the substantial circumferential pressure variations which exist in a bend dissipate almost immediately when the flow passes from the bend into the downstream-positioned straight tube. With the bend in place, the axial pressure gradients in the entrance region of the tube are smaller than the fully developed gradients at the lower Reynolds numbers and larger at the higher Reynolds numbers. A lengthwise-linear pressure variation is attained for all cases at an axial distance of 20 diameters or less from the tube inlet. Compared with the measured no-bend baseline values, the fully developed with-bend friction factors display deviations no greater than 9%, but with larger deviations (up to 18%) when compared to straight-tube correlations from the literature.

1. INTRODUCTION

WHEN A straight circular tube is fed by the fluid flow discharged from a bend, the velocity field at the tube inlet consists of secondary motions superposed on the main axial flow. Within the tube, the complex inlet-section velocity field undergoes a redevelopment, and it is expected that at sufficient downstream distances, a fully developed pipe flow will be established. The ramifications of the bend-induced velocity field on the turbulent heat transfer and pressure drop characteristics of a tube situated downstream of a bend were the subject of a two-part investigation. The heat transfer aspects of the work are reported in ref. [1], while pressure distributions and friction factors are reported here. The introduction to ref. [1] describes the phenomenological background of the problem, and that same discussion applies here. With ref. [1] as background, full attention can be given here to the specifics of the pressure drop investigation.

The plan of the research was formulated so as to vary the velocity field provided by the bend to the downstream-positioned tube. This was accomplished by varying two parameters. One of these is the bend turn angle. The other is the flow condition at the inlet of the bend. These parameters may be clarified by reference to Figs. 1(a) and (b), which portray schematic diagrams of the investigated physical situations.

In Fig. 1(a), airflow was delivered to the bend through a 30-diameters-long hydrodynamic development tube. In this case, the air entering the bend was hydrodynamically developed. In contrast, Fig. 1(b) models the situation where fluid from a large upstream plenum is drawn into the bend through a sharp-edged inlet. As shown in Fig. 1(b), a large baffle plate was used to create this type of bend inlet configuration. It is well known that flow separation occurs at a sharp-edged inlet. The two types of bend inlet conditions are, therefore, quite distinct. For bends of moderate length, such as those considered here, the differences in the bend-inlet velocity field should be felt at the bend exit and, hence, at the inlet of the straight tube downstream of the bend.

The bend turn angle is defined by the angle θ displayed in Figs. 1(a) and (b). For each of the aforementioned bend inlet conditions and for each air flow rate defined by the Reynolds number, the turn angle parameterization was extended through the range 0, 30, 60, 90, and 180 deg. Note that the 0 deg case corresponds to the absence of the bend, so that it provides a base case against which the pressure and friction factor data for the other bend angles can be compared. In addition, the base case results are compared with available pipe flow results (without a bend) with a view to validating the experimental apparatus and measurement technique. Because of space limitations, only the results corresponding to bend turn angles of 0, 90, and 180 deg are reported here. Those for 30 and 60 deg, as well as complete

NOMENCLATURE

D	diameter of test section, bend cross section, and hydrodynamic development tube	P_x	pressure at axial location x
f	friction factor, equation (3)	P_∞	pressure in laboratory ambient
f_B	Blasius friction factor correlation, equation (4)	Re	Reynolds number, $4\dot{w}/\mu\pi D$
f_0	friction factor for no-bend case ($\theta = 0$ deg)	U	mean velocity in test section
f_u	universal friction factor correlation, equation (5)	$\dot{w}$	mass flow rate
f_θ	friction factor for with-bend case	X	axial coordinate in test section.
K_p	pressure coefficient, equation (1)		

Greek symbols

θ	bend turn angle
μ	viscosity
ρ	density.

documentation of the experimental pressure distribution data, are available in ref. [2].

The Reynolds number was parametrically assigned seven values between 5000 and 80000. Results are presented here for Reynolds numbers of 5000, 10000, 24000, and 80000, with the remainder available in ref. [2].

All apparatus components along the path of the airflow had the same diameter D (and radius R). The radius of curvature R_c of the bend centerline was fixed at a value of $R_c/R = 9$.

Static pressure measurements were made at 17 axial stations in the tube downstream of the bend in the range from $X/D = 0$ to 56, where X is the axial coordinate in the tube. At each of the first seven stations (i.e. up to $X/D = 16$), three pressure taps were deployed around the circumference. For $X/D = 20$ and beyond, only the axial pressure distributions were measured.

Two types of results will be presented—pressure distributions and friction factors. The pressure distributions are included to show the extent of the circumferential variations in the initial portion of the tube and the axial development throughout the entire tube. A presentation format will be used which highlights the effect of bend turn angle on the pressure distributions.

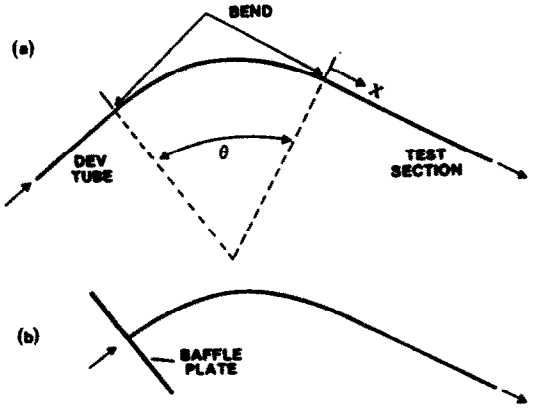

FIG. 1. Schematic representation of the two investigated bend and tube systems.

The friction factors were evaluated using pressure data in the downstream portion of the tube—from $X/D = 20$ to 56. These friction factors will be used to identify the effects of bend turn angle, bend inlet condition, and Reynolds number. Also, as already noted, the friction factors for the 0 deg turn angle are compared with the literature.

A thorough review of the open literature failed to disclose publications dealing with the pressure drop characteristics of a straight circular tube downstream of a bend, although bends, in themselves, have been well researched. Seemingly, the only reported pressure distribution measurements in a post-bend circular tube are those of Ito [3], but these were auxiliary data collected to facilitate determination of the bend pressure drop. Moreover, post-bend pressure data are reported in ref. [3] only for a single case: $Re = 2 \times 10^5$, $R_c/R = 3.7$, turn angle = 90 deg, and hydrodynamically developed flow at the bend inlet. This single pressure distribution is the only post-bend circular tube data quoted in textbooks and survey articles [4–6]. Note that the conditions of that data set do not overlap the present operating conditions, thereby precluding definitive comparisons. For noncircular cross sections, square and rectangular, there is some available pressure data in the initial portion of post-bend ducts [4].

2. EXPERIMENTAL APPARATUS AND PROCEDURE

The pressure test section tube was made of aluminum having an inside diameter of 3.175 cm (1.250 in.), a wall thickness of 0.318 cm (0.125 in.), and a finished length of 177.8 cm (70 in.), equivalent to 56 tube diameters. To remove dirt and burrs, the inside surface of the tube was thoroughly cleaned with various grades of steel wool. Next, by applying polishing compounds to the surface, and subsequently rinsing with liquid soap and water, the final surface achieved a mirror-finished quality.

The pressure test section was equipped with a total of 31 pressure taps deployed at 17 axial stations. The locations of the axial stations will be evident from the subsequent graphical presentation of the pressure distributions. To document the more significant cross-stream pressure variations, expected to occur immediately downstream of the bend exit, three pressure taps were deployed 120 deg apart around the circumference of the pressure test section tube at each of the first seven stations (i.e. up to $X/D = 16$). Figure 2 provides a key to the notation describing the circumferential locations of the taps. For $X/D = 20$ and beyond, only the axial (position B in Fig. 2) pressure distributions were measured. Fabrication of each pressure tap was initiated by drilling part way through the 3.18 mm (0.125 in.) tube wall with a 2.38 mm (3/32 in.) diameter drill bit. The pressure tap was then completed by using a number 60 drill bit (0.040 in.). Short lengths of 15-gage stainless steel tubing, inserted in each hole and epoxied in place, served as pressure tap fittings.

Upstream of the pressure test section tube, bends of 0 (no bend), 30, 60, 90, and 180 deg were used. These bends were fabricated from plexiglass, and each was made up of identical, but separate, upper and lower walls. All bends had a cross-sectional diameter D equal to 3.175 cm (1.250 in.), identical to that of the pressure test section tube. As mentioned earlier, the flow delivery to the bend was either via a hydrodynamic development tube or a sharp-edged inlet. The fabrication procedures for the bends and the inlet configurations are described in detail in ref. [2].

Downstream of the pressure test section, an exhaust tube continued the test section's 3.175 cm (1.250 in.) internal diameter for a length of about 14.5 diameters. Thereafter, it was connected to a PVC piping circuit via a vinyl hose having an i.d. of 5.08 cm (2.0 in.). Various rotameters were used for flow metering depending on the magnitude of the flow. After the rotameter, the flow passed through a control valve and was then ducted to a blower.

To avoid preheating of the air entering the apparatus, the system was operated in the open-circuit mode and in suction. The air was drawn into the apparatus from the temperature-controlled laboratory, and the compression-heated discharge from the blower was vented outside the building through the laboratory exhaust system. To eliminate the heat released from the blower to the laboratory space, the blower was housed inside a well-insulated drum. Proper auxiliary cooling for the thus-enclosed blower ensured its safe operation within the manufacturer's specified conditions.

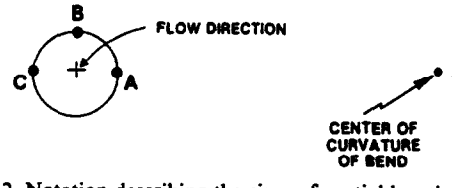

FIG. 2. Notation describing the circumferential locations of the pressure taps.

The pressure distribution in the test section tube was measured relative to the laboratory ambient pressure with electronic capacitance-type pressure transducers having pressure differential ranges of 1, 10, and 100 Torr with respective resolutions of 0.0001, 0.001, and 0.01 Torr. The manufacturer's specified accuracy for all the three sensors was 0.1% of the full scale (5 V).

To deal with the random fluctuations of the static pressure during the measurement period, a computer-assisted data acquisition procedure was employed. For a given tap, prior to the start of data taking, a period of 30 s was allowed for stabilization. Then, 100 consecutive readings were taken by the computer, averaged, and recorded as the pressure reading for that tap. With a sampling rate of 20 readings/s for the data acquisition board, it took 5 s to collect the 100 readings. To establish the aforementioned methodology, several pressure measurement tests were carried out at a random selection of taps and by varying the total number of pressure readings at each tap from 100 to 1000 with an increment of 100 (corresponding measurement times ranging from 5 to 50 s in increments of 5 s). This yielded 10 data sets (e.g. 100, 200, ..., 1000 readings). The averages for each of these 10 data sets were compared and found to vary within -0.5 to 0.3% from the base case of 100 readings in 5 s. Furthermore, for a given tap, the maximum variation among individual readings for all sets (100–1000 readings) was less than 0.9%. These findings provided justification for choosing a 30 s stabilization period and a total of 100 readings for each tap.

Execution of a pressure data run involved a number of steps which required careful attention. Prior to the initiation of a run, the ice-bath reference was readied and the thermocouple junction measuring the air temperature entering the apparatus was connected. Next, the blower(s) were activated for a warm-up period. During this period, the initial value of the barometric pressure was recorded, and the rotameters were set to the approximate desired setting. Next, depending on the run Reynolds number, the appropriate pressure sensor (1, 10, or 100 Torr) was chosen. At this point, the rotameters were checked and a final valve adjustment was made to ensure that the desired airflow rate was obtained.

Data collection was initiated by recording the rotameter reading, the pressure at the rotameter, the air temperature entering the test section, and the barometric pressure. Next, starting with tap No. 1 and following the aforementioned data acquisition procedure, the data run continued until pressure measurements for all the 31 taps were completed. The data collected during a pressure run were stored in the computer, awaiting later processing.

In addition to their initial readings, data were also collected at the middle and end of the data run for the

rotameter, the pressures at the rotameter and in the ambient, and the air temperature. Averaged values of these readings were used to calculate the mass flow rate of the air and the Reynolds number for the individual run.

3. DATA REDUCTION

The measured pressure distribution results will be presented in terms of a dimensionless pressure coefficient, defined as

$$K_p = \frac{P_\infty - P_x}{\frac{1}{2}\rho U^2} \quad (1)$$

where P_∞ is the pressure in the laboratory ambient from which air is drawn, P_x the pressure at the axial location X, and $\frac{1}{2}\rho U^2$ the velocity head. The pressure coefficient K_p will be plotted as a function of the dimensionless axial coordinate X/D for parametric values of the tube Reynolds number Re evaluated from

$$Re = 4\dot{w}/\mu\pi D \quad (2)$$

where $\dot{w}$ is the mass flow rate.

To facilitate comparison of the results with data available in the literature, a friction factor was defined as

$$f = (-\mathrm{d}P/\mathrm{d}X)D/(\tfrac{1}{2}\rho U^2) = \mathrm{d}K_p/\mathrm{d}(X/D). \quad (3)$$

The quantity $\mathrm{d}K_p/\mathrm{d}(X/D)$ is the slope of the least-squares straight line which passes through the linear portion (fully developed portion) of the K_p vs X/D plot. The experimental friction factors were compared with those of the Blasius correlation

$$f_B = \frac{0.3164}{Re^{0.25}} \quad (4)$$

and with those of the universal friction factor

$$\frac{1}{\sqrt{f_u}} = 2\log_{10}(Re\sqrt{f_u}) - 0.8. \quad (5)$$

To estimate the uncertainty levels in the experimentally determined pressure coefficients, the method proposed by Kline and McClintock [7] was used, the implementation of which is described in ref. [2].

To facilitate a unified presentation of friction factor results in which common values of the Reynolds number are used for both the tube-fed and sharp-edged cases, a slight shift of the experimental data was performed. In particular, the shift was made in accordance with the relation $f \sim Re^{-0.25}$ which follows from the Blasius equation. The shifts were generally less than 1%, so that they did not affect either the quantitative or qualitative significance of the results.

4. RESULTS AND DISCUSSION

4.1. *No-bend friction factors*

The presentation of results will begin with the friction factors corresponding to a straight tube in the absence of a bend. The experimentally determined friction factors for the no-bend case were evaluated from equation (3) and will be denoted by f_0 (the subscript 0 indicates the 0 deg turn angle). These results will be compared with the Blasius and universal friction factor correlations of equations (4) and (5) via the ratios f_0/f_B and f_0/f_u, respectively.

The comparisons are presented in Table 1 as a function of the Reynolds number for the two investigated inlet conditions, i.e. an inlet fed by a hydrodynamic development tube or a sharp-edged inlet. Note that the indicated Reynolds numbers 5000, 10 000, 24 000, and 80 000 are round numbers and are common to the two inlet configurations. This was achieved by the slight shift described in the last paragraph of Section 3.

As seen in Table 1, the present friction factors for the tube-fed case are in very good agreement with both the Blasius and universal values, with the largest deviations being in the 3% range. This level of agreement is especially significant when it is noted that both the Blasius and universal friction factor representations are, themselves, correlations of experimental data and not absolute laws. It is also noteworthy that the Kline–McClintock uncertainty estimate for the present friction factor data is about ±2.8%, which is similar in magnitude to the deviations of the data from the literature correlations.

Further inspection of the table indicates that the friction factors for the case of the sharp-edged inlet do not agree as well with the literature values as do those for the tube-fed inlet, although the deviations are still moderate. It is believed that the deviations are caused by heightened turbulence associated with the flow separation which occurs at the sharp-edged inlet. The effect appears to be greatest at the highest Reynolds number, where the region of flow separation (i.e. the recirculation zone) is most vigorous, and at the lowest Reynolds number, where the intermittency of the turbulence may have been diminished or eliminated.

Table 1. Comparison of no-bend friction factors with the literature

	Tube-fed		Sharp-edged	
Re	$(f_0/f_B)-1$ (%)	$(f_0/f_u)-1$ (%)	$(f_0/f_B)-1$ (%)	$(f_0/f_u)-1$ (%)
5000	2.1	2.7	5.7	6.2
10 000	0.7	3.2	3.0	5.4
24 000	−3.6	−1.1	−1.4	1.2
80 000	0.6	0.5	8.8	8.6

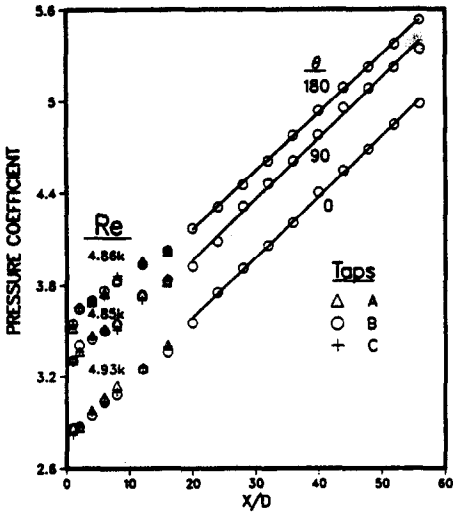

FIG. 3. Pressure distributions in a straight tube downstream of a bend fed by a hydrodynamic development section, $Re \cong 5000$.

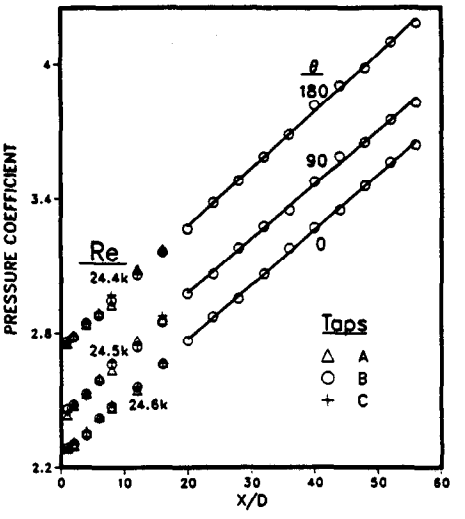

FIG. 5. Pressure distributions in a straight tube downstream of a bend fed by a hydrodynamic development section, $Re \cong 24\,000$.

4.2. *Pressure distributions corresponding to tube-fed inlet*

A graphical presentation of the axial pressure distributions for the case of the tube-fed inlet is conveyed by Figs. 3–6. In each figure, the pressure at X, expressed in dimensionless form as the pressure coefficient K_p of equation (1), is plotted as a function of the dimensionless axial coordinate X/D. Each figure corresponds to a specific nominal Reynolds number, $Re = 5000$, 10 000, 24 000, and 80 000 for Figs. 3–6, respectively. For each of these nominal Reynolds numbers, pressure distributions are plotted for three bend turn angles, 0 (no bend), 90, and 180 deg, and the individual data sets are labeled according to the turn angle. The actual Reynolds numbers for each data set are indicated in the figures.

In addition, the figures convey information on the circumferential pressure distributions. As noted earlier, data were collected at three circumferential locations, indicated as A, B, and C in Fig. 2, at the first seven axial stations (up to $X/D = 16$). The circumferential data are identified according to locations A, B, and C by the symbols shown in the legend of each figure. At axial stations beyond $X/D = 16$, data were collected only at circumferential location B.

In general, for all cases in Figs. 3–6, a linear variation of K_p with X/D appears to have been attained beginning with $X/D = 20$ (although in some cases, notably the no-bend case, the linear regime sets in earlier). The straight lines passing through the data for $X/D \geqslant 20$ are least-squares fits.

Attention will first be turned to a consideration of

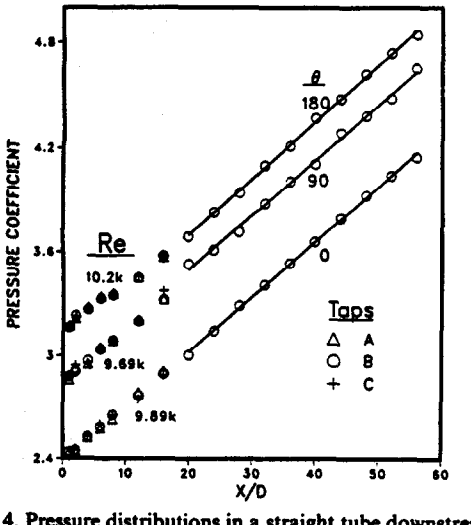

FIG. 4. Pressure distributions in a straight tube downstream of a bend fed by a hydrodynamic development section, $Re \cong 10\,000$.

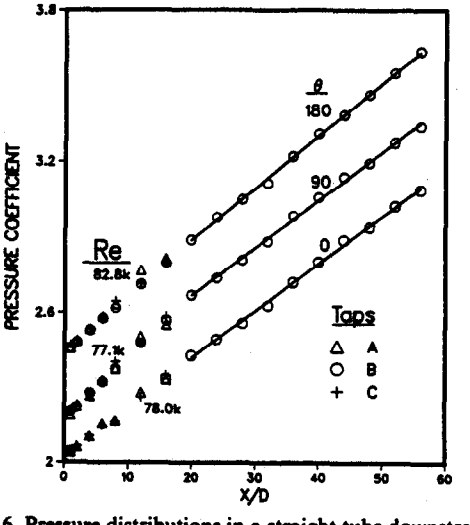

FIG. 6. Pressure distributions in a straight tube downstream of a bend fed by a hydrodynamic development section, $Re \cong 80\,000$.

circumferential pressure variations. For the no-bend case, especially in the presence of a tube-fed inlet, there is no reason to expect circumferential variations of the pressure. This expectation is confirmed by the information presented in Figs. 3–6 where, aside from normal scatter (including isolated deviations as large as 2.2%), the no-bend pressure data are circumferentially uniform.

Of even greater significance is that the circumferential pressure data in the presence of the bend display about the same degree of uniformity as do the no-bend data. This finding indicates that the substantial circumferential pressure variations which exist in a bend [8] dissipate almost immediately when the flow passes from the bend into a downstream-positioned straight tube. A similar behavior was encountered in experiments reported in refs. [4, 5] in connection with a bend and downstream duct of rectangular cross section.

Notwithstanding the just-noted rapid dissipation of the bend's circumferential pressure variation, the presence of the bend has a noticeable effect on the axial pressure distribution in the entrance region of the tube. As a benchmark, it may be noted that in the absence of the bend, the axial pressure distribution would be linear throughout the entire length of the tube as a consequence of the upstream-positioned hydrodynamic development section. Therefore, departures from pressure linearity can be ascribed to the effect of the bend.

At the lowest investigated Reynolds number ($Re = 5000$), the axial pressure gradient in the entrance region of the tube is smaller than the fully developed pressure gradient for both of the with-bend cases presented in Fig. 3. This suggests a donation of momentum from the bend-induced circumferential flow to the axial flow. A diminished entrance-region pressure gradient is also encountered at $Re = 10000$ at the largest turn angle (180 deg).

For the with-bend cases, at higher Reynolds numbers, the entrance region pressure gradient somewhat exceeds the fully developed gradient. This more conventional relationship between the gradients reflects the development of the pipe flow from the antecedent bend flow. The higher axial momentum associated with the higher Reynolds numbers trivializes possible contributions of momentum from the circumferential flow.

The final feature of Figs. 3–6 to be considered is the fully developed friction factors, the values of which are equal to the slopes of the straight lines fitted through the K_p vs X/D distributions. In any given figure among Figs. 3–6, the slopes are nearly but not precisely equal. To better examine the differences among the friction factors, Table 2 has been prepared. In the table, the friction factors for the with-bend cases, denoted by f_θ, are compared with those for the no-bend case f_0 for bend turn angles of 90 and 180 deg.

The f_θ/f_0 listing in the left-hand portion of the table pertains to the tube-fed inlet. From the table, it is seen that the friction factors for a tube situated downstream of a 90 deg bend are essentially the same as those for the no-bend case. In the presence of a 180 deg bend, the friction factors show somewhat greater deviations from the no-bend values, but the extent of the deviations is still moderate, and they may be neglected for many practical purposes. It is, however, interesting to note that the f_θ/f_0 ratio for the 180 deg turn angle increases with increasing Reynolds numbers.

Table 2. Bend-related effects on friction factors

	$(f_0/f_0)-1$ (%)			
	Tube-fed		Sharp-edged	
Re	$\theta = 90$ deg	180 deg	90 deg	180 deg
5000	−1.4	−3.7	−3.5	−5.7
10000	−2.1	1.6	−1.8	−3.2
24000	−1.6	4.6	0.5	6.7
80000	−0.8	6.1	6.2	8.6

4.3. *Pressure distributions corresponding to sharp-edged inlet*

The results for the pressure distributions corresponding to the case of the sharp-edged inlet are presented in Figs. 7–10. These figures are the counterparts of Figs. 3–6 and have the same format. As before, each figure corresponds to a specific Reynolds number in the range from about 5000 to about 80000. In reviewing and illuminating the main features of Figs. 7–10, the same issues will be addressed as were discussed in connection with Figs. 3–6.

The first issue to be considered is the possible presence of circumferential pressure variations. For the no-bend case, flow separation occurs at the inlet of the tube due to the sharp-edged configuration. If the separation and subsequent reattachment are axisym-

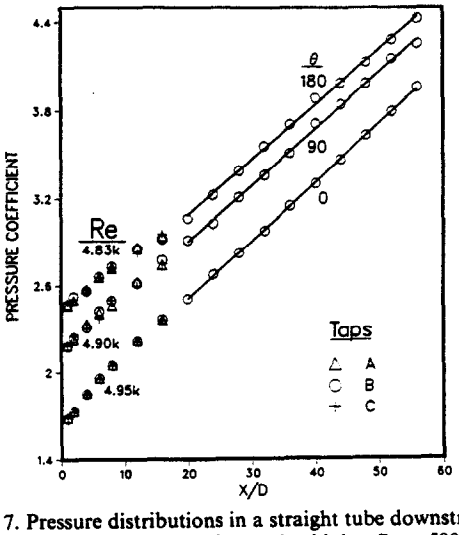

FIG. 7. Pressure distributions in a straight tube downstream of a bend fed through a sharp-edged inlet, $Re \cong 5000$.

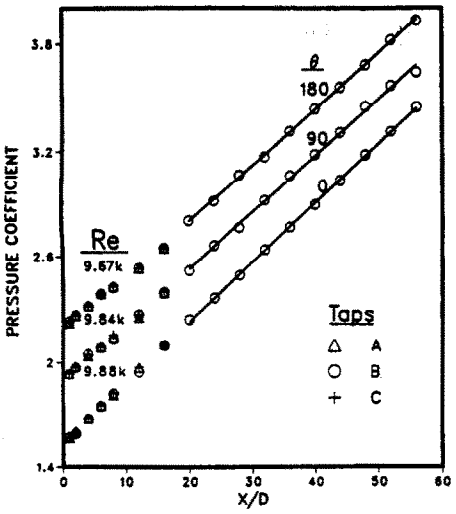

FIG. 8. Pressure distributions in a straight tube downstream of a bend fed through a sharp-edged inlet, $Re \cong 10\,000$.

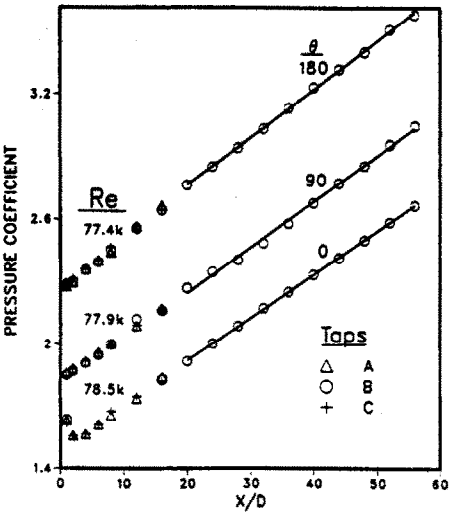

FIG. 10. Pressure distributions in a straight tube downstream of a bend fed through a sharp-edged inlet, $Re \cong 80\,000$.

metric, as should be the case for a geometrically axisymmetric apparatus, the pressure should be circumferentially uniform. This expectation is convincingly confirmed by the pressure distributions for the case of the 0 deg bend in Figs. 7–10. In the presence of the 90 and 180 deg bends, the data indicate that, aside from random scatter, circumferential uniformity of the pressure continues to prevail. This finding corroborates a similar finding for the tube-fed case and, thereby, confirms the rapid dissipation of the bend's circumferential pressure nonuniformity when the flow enters the tube.

Attention is now turned to the effect of the bend on the axial pressure distribution in the entrance region of the tube and, to begin, it is appropriate to examine the no-bend results to establish a benchmark. As already noted, in the no-bend case, flow separation occurs at the sharp-edged inlet of the tube, and a recirculation bubble is situated adjacent to the tube wall just downstream of the inlet cross section. After the separated flow reattaches to the wall, there is a hydrodynamic development which culminates in the attainment of the fully developed regime.

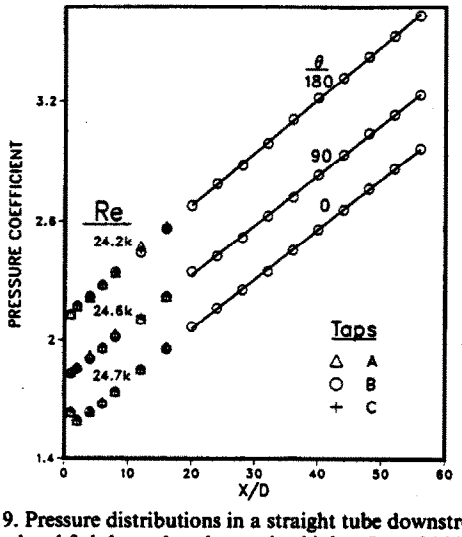

FIG. 9. Pressure distributions in a straight tube downstream of a bend fed through a sharp-edged inlet, $Re \cong 24\,000$.

At the lower Reynolds numbers, $Re = 5000$ and 10 000, no explicit imprint of the recirculation zone is evident in the pressure distribution (Figs. 7 and 8), suggesting that the recirculation zone has terminated upstream of the first measurement station in the tube. The entrance-region pressure gradient exceeds the fully developed gradient, reflecting the development of the flow. At the higher Reynolds numbers, $Re =$ 24 000 and 80 000, there is a local minimum in K_p (i.e. a local maximum in P_x) at the second pressure tap (Figs. 9 and 10). This local minimum reflects the pressure recovery which occurs downstream of the *vena contracta* of the separated flow, as the flow expands to fill the cross section of the tube. A short development length occurs downstream of the reattachment of the flow.

With a bend in place, the flow separation and reattachment occur at the inlet of the bend and not at the inlet of the tube. Therefore, none of the separation-related features in the axial pressure distributions for the no-bend case pertain when the bend is present. Instead, the entrance-region axial pressure distributions for the with-bend cases in Figs. 7–10 display similar trends as those of Figs. 3–6. Specifically, at the lower Reynolds numbers, the entrance-region pressure gradients are smaller than the fully developed pressure gradients, while at the higher Reynolds numbers, the opposite (more conventional) relationship applies. These trends have already been discussed in connection with Figs. 3–6.

The fully developed friction factors associated with Figs. 7–10 will now be considered. These friction factors are displayed in the right-hand portion of Table 2 via the f_θ/f_0 ratio, which compares the with-bend

and no-bend results. The listing indicates a common trend for both of the investigated turn angles, whereby f_θ/f_0 increases with increasing Reynolds numbers. For the lower Re, $f_\theta < f_0$, while for the higher Re, $f_\theta > f_0$. These results suggest that at lower Re, the increase in f_0 caused by the sharp-edged inlet does not occur for f_θ (because the tube is shielded from the inlet by the bend) and that the other bend-related effects on f_θ are small. At the higher Re, the bend-related increase in f_θ clearly exceeds the increase in f_0 due to the sharp-edged inlet.

With respect to practical applications, it is interesting to examine f_θ/f_B or f_θ/f_u, since f_B or f_u would, in all likelihood, be used to obtain estimates for f_θ in the absence of other information. Such an examination is facilitated by combining the results of Tables 1 and 2 for the sharp-edged-inlet case in accordance with the identity $f_\theta/f_B = (f_\theta/f_0)(f_0/f_B)$ and similarly for f_θ/f_u. The largest deviations of f_θ from f_B or f_u are about 18 and 15%, respectively for the 180 and 90 deg bends at $Re = 80\,000$. Therefore, for these cases, the f_B or f_u correlations should not be used. For the 180 deg bend at $Re = 24\,000$, $f_\theta/f_B = 1.05$ and $f_\theta/f_u = 1.08$, which is at the threshold of practical significance. For the other cases, the deviations are negligible.

5. CONCLUDING REMARKS

The experiments described here are, seemingly, the first systematic study of the effect of a bend on the pressure distributions and friction factors in a straight tube situated downstream of a bend. The pressure distribution measurements were planned so as to show the extent of the circumferential variation in the initial portion of the tube and the axial development throughout the entire length of the tube. Three parameters were varied during the experiments. These included: (1) the tube Reynolds number, which ranged from about 5000 to about 80 000, (2) the turn angle of the bend, for which results are reported here for 0, 90, and 180 deg (with the 0 deg turn angle corresponding to no bend in place), and (3) the flow delivery configuration at the inlet of the bend, either a hydrodynamic development tube or a sharp-edged inlet.

The experiments performed without a bend and with the tube fed by a hydrodynamic development section served to verify the apparatus, instrumentation, and operating procedure. The friction factors from these experiments were found to be in very good agreement with both the Blasius and universal friction factor correlations from the literature. The no-bend friction factors for the case of the sharp-edged inlet displayed moderate deviations from the literature correlations at certain Reynolds numbers, suggesting a somewhat heightened turbulence level due to the separation process which occurs at the inlet.

The installation of circumferentially deployed pressure taps in the initial portion of the tube enabled examination of the possible propagation of the bend's circumferential pressure variations into the tube. Aside from random data scatter, the pressure distributions in the tube were circumferentially uniform, indicating the virtually immediate dissipation of the circumferential pressure variations as the flow passes from the bend into the tube.

For all cases, either with or without a bend in place, a fully developed regime characterized by a lengthwise-linear variation of the pressure was attained for $X/D \geqslant 20$. With the bend in place and for the lower Reynolds numbers (5000 and 10 000), the entrance-region pressure gradients were found to be smaller than the corresponding fully developed pressure gradients. At higher Reynolds numbers, the opposite (more conventional) relationship between the entrance-region and fully developed gradients existed.

The presence of a bend did not affect the fully developed friction factors for the tube-fed case for a 90 deg bend angle. However, for all the other investigated cases, the ratio of the with-bend to the no-bend friction factors increased with increasing Reynolds numbers, with a maximum value of the ratio of about 1.09. Compared with the friction factors from the Blasius or the universal correlation, deviations of the measured with-bend friction factors as large as 18% were noted, specifically for the sharp-edged-inlet case and for the 180 deg bend turn angle at $Re = 80\,000$.

REFERENCES

1. M. M. Ohadi and E. M. Sparrow, Heat transfer in a straight tube situated downstream of a bend, *Int. J. Heat Mass Transfer* **32**, 201–212 (1989).
2. A. Walavalkar, Turbulent heat transfer and pressure drop characteristics in a straight circular tube situated downstream of a 180 degree bend, M.S. Thesis, Department of Mechanical Engineering, Michigan Technological University, Houghton, Michigan (1988).
3. H. Ito, Pressure losses in smooth pipe bends, *J. Basic Engng* **82**, 131–143 (1960).
4. A. J. Ward Smith, *Pressure Losses in Ducted Flows*. Butterworths, London (1971).
5. A. J. Ward Smith, *Internal Fluid Flow*. Clarendon Press, Oxford (1980).
6. S. A. Berger, L. Talbot and L. S. Yao, Flow in curved pipes, *A. Rev. Fluid Mech.* **15**, 461–512 (1983).
7. S. J. Kline and F. A. McClintock, Describing uncertainties in single-sample experiments, *Mech. Engng* **75**, 3–8 (1953).
8. G. M. Chrysler and E. M. Sparrow, Turbulent flow and heat transfer in bends of circular cross section: II—pressure distribution experiments, *J. Heat Transfer* **108**, 212–216 (1986).

CARACTERISTIQUES DE PERTE DE CHARGE POUR UN ECOULEMENT TURBULENT DANS UN TUBE RECTILIGNE, A SECTION CIRCULAIRE, EN AVAL D'UN COUDE

Résumé—Des expériences sont faites pour quantifier les effets d'un coude sur les distributions de pression et de coefficient de frottement dans un tube rectiligne situé en aval d'un coude. Des résultats sont reportés pour des valeurs paramétriques du nombre de Reynolds (5000–80 000), de l'angle de coude (0,90 et 180°) et de configuration d'écoulement à l'entrée du coude (soit un écoulement hydrodynamique établi soit une entrée à bord mince). L'angle de cintrage de 0° correspond à l'absence de coude, ce qui sert de référence pour les autres cas. On trouve que les variations circonférentielles de pression qui existent dans un coude se dissipent presque immédiatement au-delà. Avec le coude en place, les gradients axiaux de pression dans la région d'entrée du tube sont pour les petits nombres de Reynolds plus faibles que les gradients pleinement établis mais plus grands pour les nombres de Reynolds plus élevés. Une variation de pression linéaire est obtenue dans tous les cas à une distance axiale de 20 diamètres ou moins, à partir de l'entrée du tube. En comparaison du cas sans coude, les coefficients de frottement ne s'écartent pas plus de 9%, mais avec des déviations plus importantes (jusqu'à 18%) en comparaison des données de la littérature pour le tube rectiligne.

DRUCKABFALL BEI TURBULENTER STRÖMUNG IN EINEM KREISFÖRMIGEN GERADEN ROHR HINTER EINEM ROHRKRÜMMER

Zusammenfassung—Der Einfluß eines Rohrkrümmers auf die Druckverteilung und den Reibungsbeiwert in einem stromabwärts anschließenden geraden Rohrstück wird experimentell untersucht. Es werden Ergebnisse für verschiedene Reynolds-Zahlen (5000 bis 80 000), Krümmungswinkel (0°, 90°, 180°) sowie unterschiedlich ausgeführten Strömungseinlaß am Krümmer dargestellt (hydrodynamisch entwickelte oder scharfkantige Zuströmung). Der Krümmungswinkel 0° entspricht dem Fall ohne Krümmer und wird als Vergleichsgrundlage für die anderen Versuche verwendet. Wie sich zeigt, lösen sich die Druckunterschiede am Rohrumfang, die innerhalb der Krümmung beträchtlich sind, schnell nach dem Einströmen in das gerade Rohrstück auf. Bei vorhandenem Krümmer sind die axialen Druckgradienten in der Einlaufzone des Rohres bei niedrigen Reynolds-Zahlen geringer als die Druckgradienten der voll ausgebildeten Strömung, bei hohen Reynolds-Zahlen größer. In Längsrichtung der Strömung wird in allen Fällen in Abständen von 20 oder weniger Rohrdurchmesser vom Rohreinlaß eine lineare Druckverteilung erreicht. Verglichen mit den Messungen ohne Krümmer zeigen die Reibungsfaktoren der voll ausgebildeten Strömung mit Krümmer Abweichungen unter 9%. Abweichungen der Messungen zu aus der Literatur entnommenen Berechnungsgleichungen für Strömungen in geraden Rohren steigen jedoch hier bis zu 18%.

ПЕРЕПАД ДАВЛЕНИЯ ПРИ ТУРБУЛЕНТНОМ ТЕЧЕНИИ НА ПРЯМОМ УЧАСТКЕ КРУГЛОЙ ТРУБЫ ЗА ИЗГИБОМ

Аннотация—Проведены экспериментальные исследования для количественной оценки влияния изгиба на распределение давления и коэффициенты трения на прямом участке трубы, расположенном вниз по течению за изгибом. Получены результаты при заданных значениях числа Рейнольдса (5000–80 000), угла изгиба (0, 90, и 180°) и при определенной подаче потока на вохд изогнутой части (гидродинамически развитое течение или вход с острой кромкой). Угол поворота потока в 0° соответствовал отсутствию изгиба, и значения для этого случая служили основой для сравнения с полученными результатами. Найдено, что существенные изменения давления по окружности трубы в месте изгиба почти мгновенно исчезают при переходе потока в прямую трубу за изгибом. При правильном расположении изогнутой части аксиальные градиенты давления в области входа в трубу ниже градиентов полностью развитого потока при меньших значениях числа Рейнольдса и выше при более высоких его значениях. Во всех из исследованных случаев получено линейное изменение давления по длине трубы на расстоянии, равном 20 диаметрам трубы от ее входа и менее. Коэффициенты трения для полностью развитого течения с изгибом отклонялись от контрольных значений без изгиба не более чем на 9% и на 18% от значений, рассчитываемых по соотношениям, используемым в литературе для прямой трубы.